Sensors and Actuators A 318 (2021) 112492

Contents lists available at ScienceDirect

Sensors and Actuators A: Physical

journal homepage: www.elsevier.com/locate/sna

A high-temperature resistant photonic crystal fiber sensor with single-side sliding Fabry-Perot cavity for super-large strain measurement

Ping Xia, Yuegang Tan, Tianliang Li *, Zude Zhou, Wenqiang Lv

The School of Mechanical and Electronic Engineering, Wuhan University of Technology, Wuhan, China

ARTICLE INFO

Article history:
Received 2 July 2020
Received in revised form
18 November 2020
Accepted 7 December 2020
Available online 10 December 2020

Keywords:
Photonic crystal fiber
Fabry-Perot
Super-large strain
High-temperature

ABSTRACT

A photonic crystal fiber (PCF) Fabry-Perot (F-P) sensor capable of super-large strain measurement under high temperatures has been proposed and investigated in this paper. Two PCFs have been inserted inside of both sides of a quartz capillary with laser welding fixed and freely suspended layouts, respectively. Such configuration leads to a single-side sliding F-P cavity with a large measurement range. The designed sensor is compact and support a simple fabrication procedure with low cost. The sensing principle and validation experiments have been derived and implemented, respectively. Experiments results demonstrate that the sensor has an excellent resistance for the temperature within the range of 28 ^{o}C ~ 1100 ^{o}C. A large mechanical-induced strain of 9436.66 $\mu\varepsilon$ can be accurately detected under a high-the temperature reaching 1000 ^{o}C. These merits enable the designed sensor to detect the super-large strain of turbine blades under a high-temperature environment.

© 2020 Published by Elsevier B.V.

1. Introduction

Most of mechanical equipment such as aero engines and gas turbines typically works under extremely high temperature in excess of 1000 °C, strong electromagnetic interference, high rotation speed and high pressure environment. Such case generally results in a super-large strain on some key components such as turbine blades and combustors [1,2]. Strain is an important parameter to assess the safety and health of mechanical equipment [3–5], which can effectively reflect fatigue and damage status of them [6,7]. Therefore, it is significant to develop a super-large strain sensor for monitoring health state of the mechanical equipment under high-temperature environment.

At present, the stability and accuracy of the traditional electrical-sensors are difficult to satisfy the above-mentioned requirements due to electromagnetic interference. Meanwhile, they are prone to failure under the above high temperatures [8]. However, fiber-optic sensors can effectively address these drawbacks due to their inherent properties such as electromagnetic immunity, high temperature, corrosion resistance, and remote multiplex capacity [9,10], and they find important application in civil structure health monitoring, mechanical equipment and robot, etc [11]. Besides, their advantages of small size, low weight and geometric flexibility enable their easy installation or embedment to test body with less influence on the status of the running equipment [5,12,13]. Therefore, optical fibers are adopted with attempts to develop strain sensors which are mainly intensity-based [13], grating-based [12,14], and interferometric [15]. Measurement accuracy of the intensity-based sensors is easily affected by source fluctuation, bending of the fiber and the connection loss [13]. Fiber Bragg gratings (FBGs) which are demodulated by the center wavelength without effects from power fluctuation of optical source and the variations of fiber losses have aroused more attention. At early stages, the normal UV-induced FBGs (Type I) have been employed to design strain sensors. The typical tensile strain limit of this type of FBG is less than 4000 $\mu\varepsilon$ (~0.4 %) [16]. However, when UV-inscribed FBGs are exposed to temperature higher than 300 °C, thermal decay will occur resulting in FBG's degradation and failure [16]. Although the thermal stability of the regenerated FBGs (RFBGs) and Type II femtosecond FBGs (fs-FBGs) are up to 1295 ^{o}C [17,18] and ~ 1000 °C [19,20], they are brittle and fragile [21] resulting in packaging difficulties for strain sensor development.

Recently, some fulfilments based on optical fiber Fabry-Perot (F-P) interferometers have been widely employed to design strain sensors compared with the other optical fiber sensing techniques due to simple fabrication and compact package structure [22]. Rao

* Corresponding author at: The School of Mechanical and Electronic Engineering, Wuhan University of Technology, Wuhan, China.
E-mail addresses: xiaping525@163.com (P. Xia), ygtan@whut.edu.cn (Y. Tan), tianliangliwhut@sina.com (T. Li).

https://doi.org/10.1016/j.sna.2020.112492
0924-4247/© 2020 Published by Elsevier B.V.

et al. proposed the configuration of in-line cavity formed by splicing a section of hollow-core photonic crystal fiber (HCPCF) between two single-mode fibers (SMFs), this sensor has been demonstrated to measure strain up to 1200 με [23]. A different type of F-P strain sensor obtained by splicing a SMF to a HCPCF tip were presented by Deng group, which was demonstrated to measure 1850 με [15]. Air cavity-based FPIs with different shapes such as a micro-bubble [24] or a spheroidal cavity [25] were fabricated inside the fiber and used as strain sensors. Liu et al. proposed the formation of a rectangular air bubble by splicing together two sections of SMFs and tapering the splicing joint. Such a F-P strain sensor has a very high strain sensitivity of 43.0 pm/με (Note: pm/με denotes that each mircostrain can induce one picrometer shift of scanning wavelength of the F-P interference spectrum) and a relative low thermal sensitivity of 2.0 pm/°C, and was demonstrated to measure 450 με [26]. All -silica micro-machined fiber taper cavity F-P strain sensor [27,28] has been developed to improve the sensitivity. Nevertheless, it involves a complex manufacturing process, and was not discussed the effect of large-strain measurement under high temperature. However, the strain measurement principle of the aforementioned configurations is based on elongation or deformation of the sensor head, in which the tensile strength of the sensor head limits the strain range. Since the strength of fiber is greatly damaged after being processed, the above sensors can only measure a small amount of strain.

This paper presents a photonic crystal fiber (PCF) F-P super-large strain sensor with an excellent temperature resistance. This sensor comprises of two PCFs and a capillary tube with the material of pure SiO_2. Unlike conventional SMFs which entail a doped core surrounded by a pure silica cladding, PCFs present a solid core or a hollow core without dopant surrounded by a periodic array of microscopic air holes, which leads to an excellent high-temperature resistance [29]. Two PCFs are inserted and deployed at both sides of the capillary tube. One connect between PCF and the tube is fixed by laser welding, but the other connect is free. This delicate configuration forms a single-side sliding F-P cavity which supports a large strain measurement. The sensing principle, sensor fabrication and theoretical model have been introduced and derived, respectively. The temperature and tensile testing have been conducted, which effectively verify the feasibility of the designed sensor for measuring the super-large strain under high temperatures.

2. Sensor fabrication and measurement principle

2.1. Sensor fabrication

The schematic of working principle of the proposed F-P strain sensor is shown in Fig. 1 (a). The designed sensor mainly consists of two PCFs (Company: YOFC, China; Type: PC SM 1010-A) with the diameter of 125 μm and a capillary tube for alignment and protecting the closed F-P cavity. Such a tube with inner diameter of 128 μm is made of pure quartz which can sustain temperature up to 1450 °C. The quality of F-P interference spectrum is closely associated with the flatness of the both end faces of the F-P cavity. Thus, both PCFs have been cleaved by an optical fiber cleaver (Company: SUMITOMO ELECTRIC, Japan; Type: FC-6S) to achieve smooth flat end-face firstly. The two end faces are labeled as reflective surface I and II, respectively. Subsequently, both PCFs have been inserted into the capillary tube. The initial distance between the two end faces is configured with 196 μm to form the F-P cavity. Right PCF is spliced to the capillary tube by laser welding instead of glue which can avoid some adverse effects of glue creep and mismatch of coefficient of thermal expansion (CTE) between glue and pure quartz. The cross-sectional view of PCF and optical microscope image of the

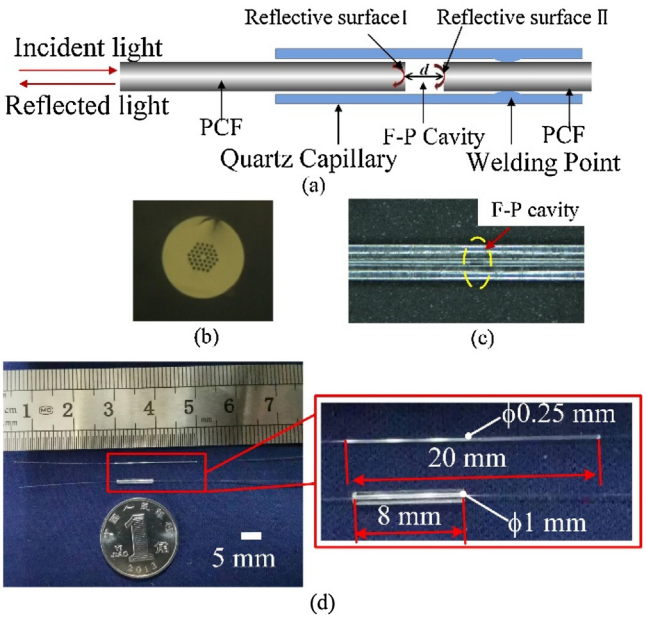

Fig. 1. (a) Schematic of the proposed sensor; (b) the cross-sectional view of PCF; (c) microscopic image of the sensor head; (d) the prototyped F-P strain sensor.

designed sensor head are displayed in Fig. 1(b) and (c) respectively. The interference spectrum of F-P cavity is real-time demodulated by an interrogator (Fabricated by Wuhan University of Technology; cavity length resolution: 10 nm). Two prototyped sensors have been fabricated. Their lengths are 8 mm and 20 mm, as shown in Fig. 1 (d).

2.2. Measurement principle

From the Fig. 1(a), when a board-band light incidents into the left PCF, the light will be reflected from end-faces of the two PCFs and interfere with each other. Optical spectrum of the F-P interferometric sensor can be expressed as [30]:

$$g(\lambda) = a(\lambda) + b(\lambda) \cdot \cos(\varphi + \pi) \tag{1}$$

$$\varphi = \frac{4\pi d}{\lambda} \tag{2}$$

where $a(\lambda)$ and $b(\lambda)$ are the background spectral profile of light source and the interference fringe contrast, respectively. φ is the phase of interference fringe, λ denotes the scanning wavelength, d is the cavity length of F-P sensor. The F-P cavity length is detected by the white-light interferometry demodulation technology. With wavelength scanning from λ_1 to λ_2, there is a phase change of $\Delta\varphi$ in the F-P interference fringe. The relationship between $\Delta\varphi$ and d is determined as,

$$\Delta\varphi(\lambda) = \varphi(\lambda_2) - \varphi(\lambda_1) = \frac{4\pi d(\lambda_2 - \lambda_1)}{\lambda_1\lambda_2} \tag{3}$$

Phase change $\Delta\varphi$ can be determined by Fourier transforming the measured optical spectrum. Thus, the cavity length d is to be calculated by the phase change $\Delta\varphi$, as follows:

$$d = \frac{\lambda_1\lambda_2}{4\pi(\lambda_2 - \lambda_1)}\Delta\varphi(\lambda) \tag{4}$$

For strain measurement, the sensor head needs be pasted to the measured target by the use of adhesive, as shown in Fig. 2. The input PCF is rigidly fixed on the measured target. The capillary tube bonded with the right PCF is mounted on the measured target, as well. During strain measuring, the input PCF will slide along

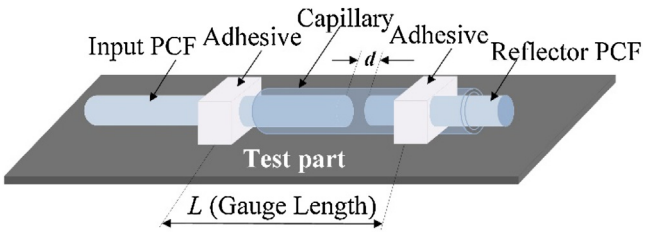

Fig. 2. Concept diagram of the sensor pasted to test part.

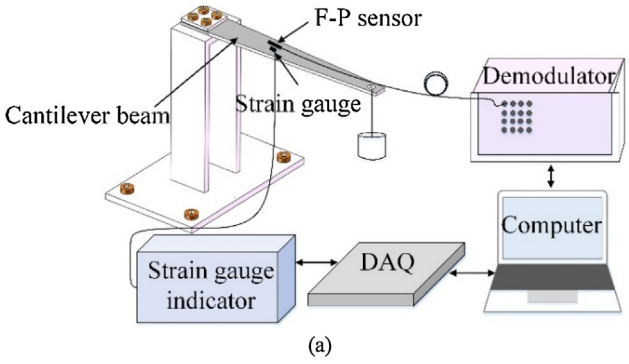

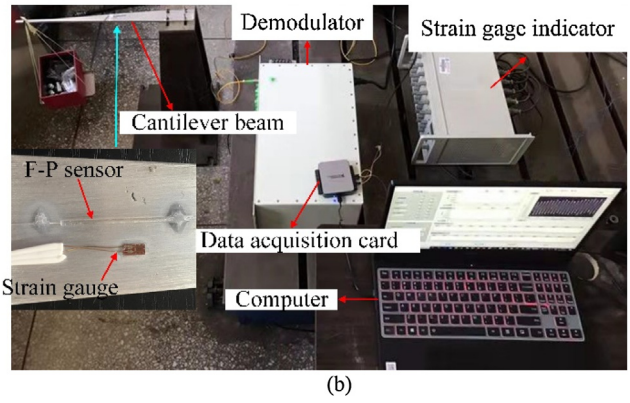

Fig. 3. (a) Schematic diagram for strain test at room temperature; (b) Experimental setup for strain test at room temperature.

the capillary tube. The corresponding cavity length of the F-P sensor will be changed. According to the mechanics of materials, the sensed strain of the designed sensor can be formulated as:

$$\varepsilon = \frac{\Delta d}{L} = \frac{d' - d}{L} \tag{5}$$

$$d' = L\varepsilon + d \tag{6}$$

where d is the original cavity length of the sensor, d' is the cavity length after deformation, L is the initial gauge length before deformation, which represents the distance between the two adhesive positions. The strain sensitivity of the sensor can be adjusted by the original sensor gauge length L.

3. Experimental setup

3.1. Strain calibration experiments

To calibrate the sensing properties of the designed sensor, the experimental system has been established, as shown in Fig. 3. This system comprises of an equal-strength cantilever beam, the designed strain sensor and a commercial resistance strain gauge

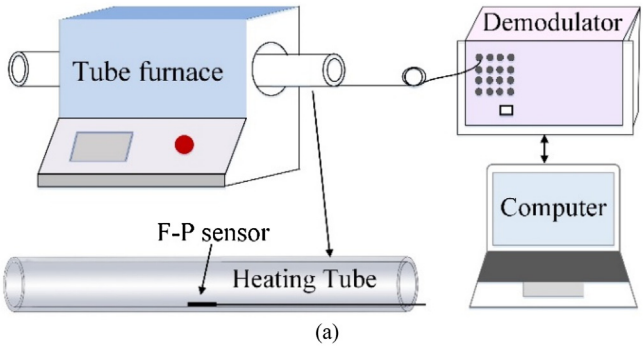

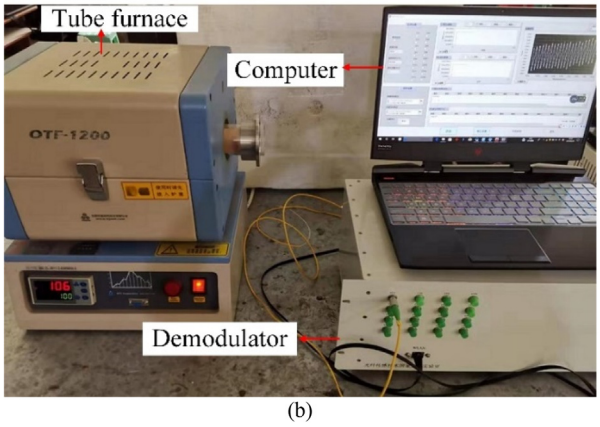

Fig. 4. (a) Schematic diagram for temperature test; (b) Experimental setup for temperature test.

utilized as a reference. The designed sensor with the gauge length of 25 mm and the commercial strain gauge are pasted on beam by the use of polyimide-based adhesive. Their positions are very close, as shown in Fig. 3(b). For static strain measurement, the weights loaded at the end of the beam were increased from 0 g to 500 g and decreased back to 0 g in steps of 50 g. Such a procedure was repeated 3 times. Signals of the designed sensor and the commercial strain gauge were acquired by F-P demodulator and a strain gauge indicator (Beidaihe institute of electronics; SDY2101) during the calibration experiments.

To investigate dynamic measurement capability of the designed sensor, a variable load with a frequency of 30 Hz has been applied on the cantilever beam arranged with the designed sensor and a commercial strain gauge. The real-time response of the designed sensor and commercial strain gauge were recorded in the experiment.

3.2. Temperature testing experiments

The high-temperature experiments have been established to investigate the temperature resistance of the designed sensor, as shown in in Fig. 4. The designed sensor is freely placed inside a high-temperature tube furnace (Company: KE JING, China; Model: OTF-1200X). Such a furnace was used to control the temperature from 100 °C to 1100 °C in a step of 100 °C. The temperature was kept constant for 30 min at each step before recording the data to avoid the effect of temperature fluctuation and non-uniform distribution.

Additionally, the stability of the designed sensor under high temperatures is a significant factor when using it to measure high-temperature strain. In this case, the designed sensor was fixed on a 304 stainless steel plate, and then put them together inside the heating tube. When the temperature is increasing, a thermal strain is to be generated on the surface of the steel plate. Such a result leads to a corresponding increase of the cavity length. The temperature implementation was within the range of 100 °C∼ 600 °C. Based on

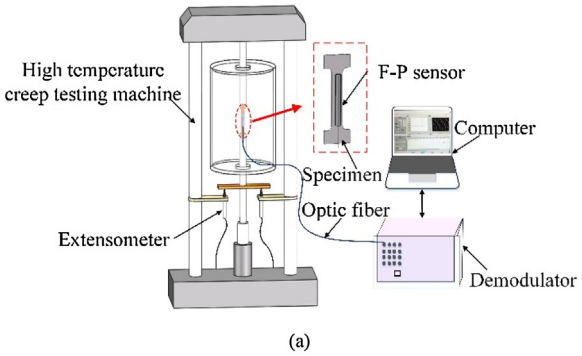

(a)

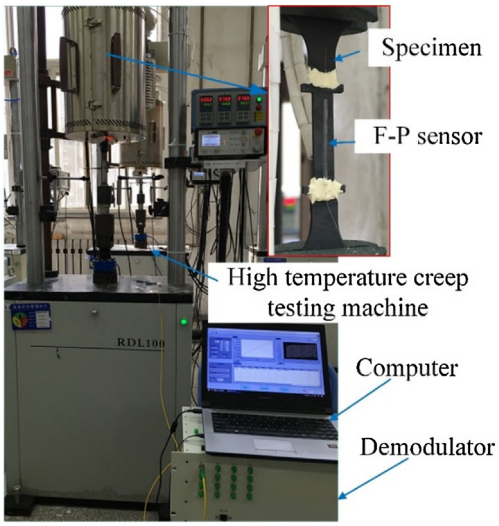

(b)

Fig. 5. (a) Schematic diagram for high temperature strain test; (b) Experimental setup for high temperature strain test.

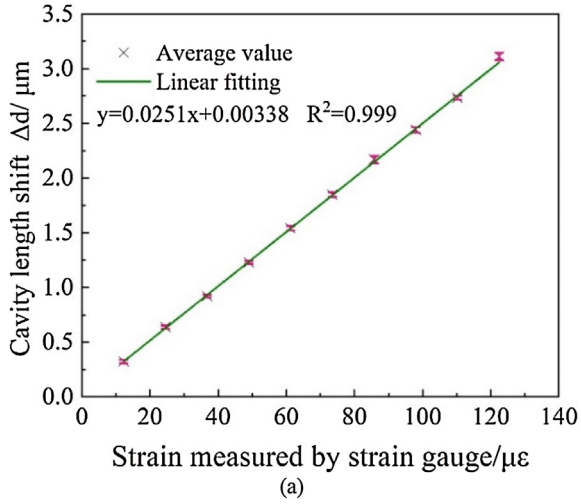

(a)

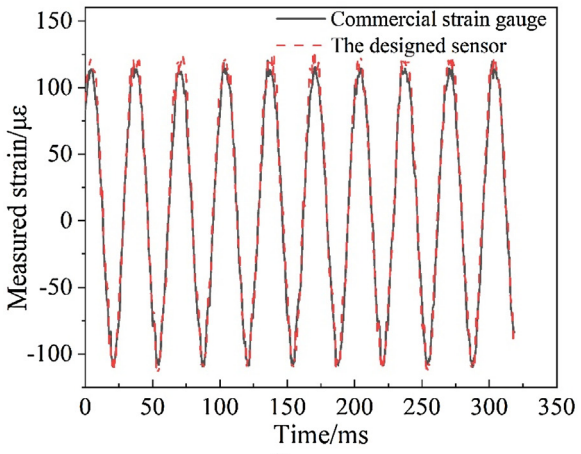

(b)

Fig. 6. (a) Cavity length shift (Δd) of the designed sensor versus reference strain captured from the commercial strain gauge; (b) Comparison dynamic measurement result between the designed sensor and a commercial strain gauge.

the above operations, the stability of the designed sensor can be evaluated under high-temperature environment. This experiment was repeated three times.

3.3. Verification experiments for high-temperature super-large strain measurement

To further evaluate super-large strain capability of the designed sensor under high temperatures, an experimental system based on a high-temperature creep testing machine (Company: ZHONG JI, China; Model: RDL 100) has been built, as illustrated in Fig. 5. This testing machine can provide a large load of up to 100 kN under high temperatures. Before testing, the designed F-P sensor with original cavity length of 149 μm and gauge length of 31 mm was mounted on a K405 specimen (Length: 96 mm, Width: 5 mm, Thickness: 2 mm) by the ZrO_2-based (Resbond 904, Company: Cotronics, USA) adhesive, as displayed in Fig. 5(b). The K405 metal is nickel-base cast superalloy which is generally used for making gas turbine blades and other hot components. The specimen was fixed on the testing machine. During experiment, the temperature increased to 1000 ºC first without load. Then a variable load that is increasing to 4 kN at a constant speed of 2 kN/min has been imposed on the specimen under the constant temperature of 1000 ºC to further investigate the maximum strain measurement capability of the designed sensor. The response of the designed sensor is recorded by the demodulator.

4. Experimental results analysis

4.1. Results of strain calibration experiments

The cavity length shift (Δd) of the designed sensor versus reference strain captured from the commercial strain gauge is shown in Fig. 6(a). Both ascending and descending load have been repeated three cycles, respectively. The error bars in the vertical axes at each strain value represent the standard deviation for the measured average cavity length shifts between test repetitions. The fitted line for the average values of six experimental data can be achieved by using the least-squares method, which shows an excellent linearity of 0.99995 with an R2 = 0.999. The sensitivity of the designed F-P strain sensor is 0.0251 μm/με. The real-time response of the sensor under a dynamic load with a frequency of 30 Hz can be calculated by the fitted equation in Fig. 6(a), which is displayed in Fig. 6(b). Compared with the commercial strain gauge, the maximum relative error of the designed sensor is 6.77 %.

4.2. Results of temperature testing experiments

Interference spectrum of the designed sensor under different temperatures (28 ºC ~ 1100 ºC) is captured from the demodulator, as illustrated in Fig. 7(a). This figure shows that the peak shifts to the right and the cavity length increases as the temperature increases.

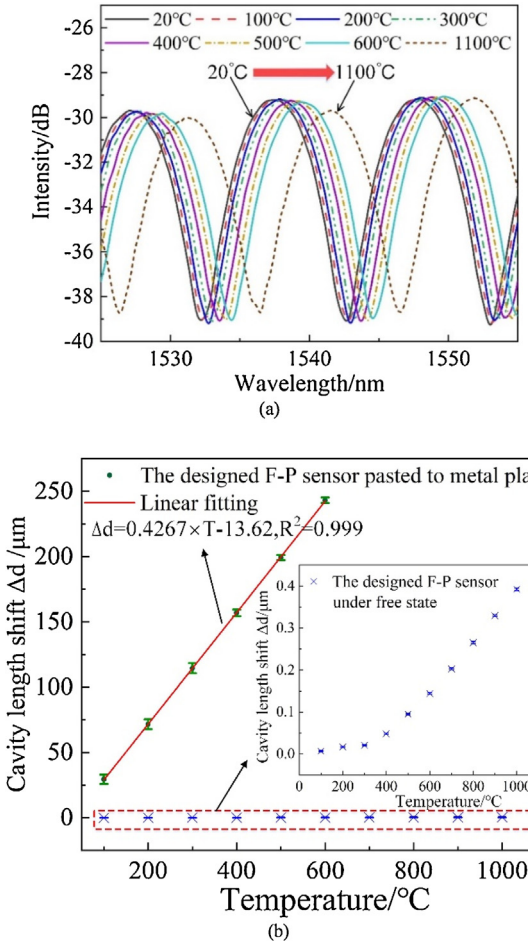

Fig. 7. (a) Interference spectrum of the designed sensor under different temperatures; (b) the relationship between cavity length shift (Δd) of the designed sensor and the applied temperature.

The related relationship between cavity length shift (Δd) of the designed sensor and the applied temperature with a small nonlinear variation is displayed in the subfigure of Fig.7 (b). Such a nonlinear variation is caused by the inconsistent thermal expansion coefficients of SiO_2 under different temperatures [31,32]. The maximum value of the cavity length shift is less than 0.3611 μm when the temperature is up to 1100 °C. The relationship between cavity length shift (Δd) of the designed sensor and the applied temperature is obtained in Fig. 7 (b) when the designed F-P sensor is mounted on the stainless-steel plate to measure the thermal strain. As observed from the figure, the response curves show a good repeatability and linearity within the range of 28 °C ~ 600 °C. The temperature-induced strain sensitivity of the plate can be obtained from the linear fitted equation, which is 0.4267 μm /°C.

4.3. Results of verification experiments for high-temperature super-large strain measurement

When the temperature reached 1000 °C, the cavity length increased to 534 μm. The corresponding thermal strain can be calculated by the Eq. (5), which is up to 1.24 × 10^4 με. With the applied tensile load under the temperature of 1000 °C, the cavity length increases with the increase of applied force. The stress of the specimen can be calculated which is equal to the rate between the applied force and its cross-sectional area. The mechanical-induced strain of the designed sensor can be also determined by Eq. (5). Consequently, the relationship between the stress and the sensed strain can be obtained, as shown in Fig. 8. From this figure, the maximum sensed strain is about 9436.66 με under the applied stress of 400 Mpa without fracturing the specimen. In this experiment, the maximum strain detection value of the designed sensor can be calculated, which is equal to the sum of the thermal and mechanical-induced strain. It is up to 2.18 × 10^4 με.

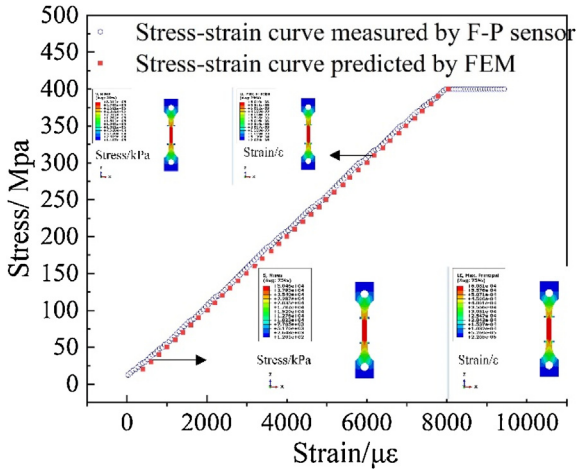

Fig. 8. Corresponding response curves of the strain-stress relationship for the designed sensor and FEM simulation under a constant temperature of 1000 °C.

Additionally, to further validate the correctness of the detected strain, the stress and strain of the tensile specimen with respect to the applied dynamic loading has been simulated under temperature of 1000 °C by using the finite element method (FEM) in ABAQUS, as shown in Fig. 8. Since the mechanical properties of K405 vary from room temperature (30°C) to high temperature, these variations have been considered in the FEM model to properly predict the response of the specimen at high temperature. As observed from Fig. 8, the curve determined from the sensed strain is basically consistent with the simulation results. Such results illustrate the correctness and effectiveness of the designed sensor for measuring the super-large strain under high-temperature environment.

5. Discussions and conclusion

A PCF sensor based on F-P interferometer is capable of super-large strain measurement under high-temperature environment is presented. A closed cavity is designed by two PCFs with a smooth flat end-face and a pure quartz capillary tube with a high-temperature resistance. Two PCFs have been welded with the tube and suspended inside the tube respectively to form a single-side sliding F-P cavity. Such a configuration leads to a high range for strain measurement, small size and uncomplicated encapsulation. The parameters of the proposed sensor can be adjusted to satisfy different kinds of applications.

The fabrication procedures and sensing principle model have been introduced and derived. The designed sensor has been characterized in Fig. 6 (a). This figure illustrates that the designed sensor has a good linearity for measuring strain. The experimental sensitivity is 0.0251 μm/με. According to Eq. (6), the theoretical strain sensitivity of the designed sensor is 0.025 μm/με, which is in agreement with the experimental value. Such merits effectively validate the correctness of the theoretical sensing model of the designed sensor. The dynamic performance of the designed sensor was evaluated in Fig. 6(b). It can be seen that the captured result of the designed sensor is consistent with the commercial strain gauge, which can effectively validate the dynamic measurement capability of the designed sensor.

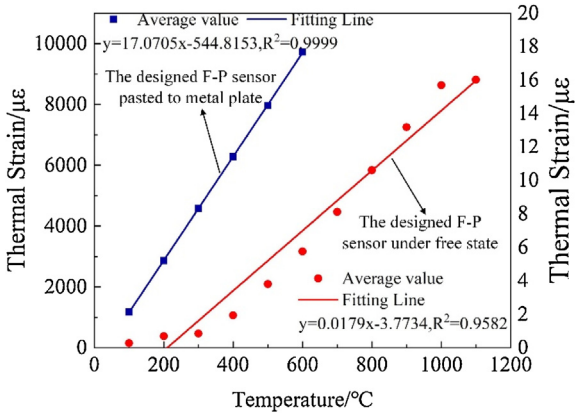

Fig. 9. The fitted line of the thermal strain-temperature relationship from the experimental data in Fig. 7 (b).

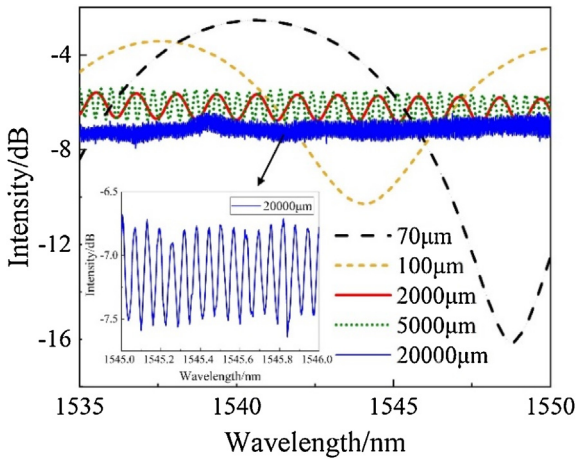

Fig. 10. The interference spectrum of F-P sensors with different cavity length.

The high-temperature resistance of the designed sensor has been investigated in Fig. 7. Signal of the designed sensor can be perfectly captured when the temperature is up to 1100 °C. It shows the excellent high-temperature capability of the designed sensor. However, there is a small fluctuation along with the temperature increase due to the thermal expansion of the capillary tube. The cavity length-temperature sensitivity is about 3.08×10^{-4} μm/°C. To further analysis, the temperature resistance of the curve of the strain-temperature relationship for the designed sensor can be calculated by using the Eq. (5), as shown in Fig. 9. As well, the curve of the strain-temperature relationship can be also obtained when the designed sensor is pasted on a stainless steel plate in Fig.7 (b), as shown in the left vertical axis of Fig.9. The thermal-induced strain sensitivity under these two cases are 17.07 με/°C and 0.0179 με/°C, respectively. The temperature cross-sensitivity of the designed sensor is about 0.0179/17.07 = 0.104 %, which is very small. Such results fully demonstrates an excellent temperature resistance of the designed sensor for large strain measurement under high-temperature environment.

In this paper, the key contributions of the designed sensor are the capabilities of large strain sensing and excellent high temperature resistance rather than distinguish the thermal and mechanical-induced strain. How to distinguish the thermal and mechanical-induced strain will be considered in the future work by configuring a hybrid sensor, such as inscribing a femto-FBG [3] in the input PCF used for measuring temperature. The curve of the strain-stress relationship detected from the designed sensor is in agreement with the simulation. Such results validate the feasibility and effectiveness of the designed sensor for measuring super-large strain under high-temperature environment. Combining with the detected maximum mechanical-induced strain of 9436.66 με in Fig. 8, the maximum strain value of the designed sensor can be determined, which is up to 2.18×10^4 με. To further ensure the maximum measured value of the strain, the interference spectra of F-P sensors has been recorded under different cavity lengths, as shown in Fig. 10. From Fig. 10, it can be seen that the interference fringe contrast and the period of the fringe decrease with the increment of the cavity length. Such a result leads to that the reflection spectrum of the designed sensor could be submerged in the Rayleigh scattering light of the fiber, and the demodulation error of the sensor increases along with the increment of the cavity length. In Fig. 10, the peak-to-peak intensity decreases to 1 dB when the cavity length is 20 mm. Therefore, the maximum strain of the designed sensor can be calculated according to the above-ground truths and Eq. (5), which is 7.92×10^5 με. Such merit leads to that the designed sensor can be used to measure super-large strain and can be also used to detect displacement.

Table 1
Performance comparison of the designed sensor and the current optical fiber large-strain sensors.

Research Group	Sensing Principle	Maximum Working Temperature	Maximum strain measurement (με)
Habisreuther, et al [7]	Sapphire Fibers FBG	600 °C	1500
Deng, et al [15]	Micro air bubble FPI	750 °C	1850
Rao, et al [23]	In-line FP etalon	100 °C	1200
Favero, et al [25]	Spheroidal air cavity FPI	100 °C	1000
Liu, et al [26]	Rectangular air bubble FPI	100 °C	450
Simon, et al [28]	fiber taper micro-machined cavity	650 °C	3000
This paper	**A single-side sliding F-P cavity**	**1100 °C**	**2.18×10^4**

The detailed performance comparison of the existing optical fiber-based strain sensors and the designed sensor has been summarized in Table 1. The maximum working temperature and maximum strain measurement value of the designed sensor are far larger than the other mentioned strain sensors. Compared with the best temperature resistance strain sensor [15], the working temperature of the designed sensor increases to 1100 °C. Similarly, its maximum strain measurement value is 11.57 times larger than [15].

Future works will involve attachment methods/processes for the designed sensor under high temperature such as spray and welding. Such methods will be developed to ensure a reliable connect between the designed sensor and the measured object under severe environments including high temperature, vibration and air scour, etc. Meanwhile, the related attaching parameters will be investigated and optimized to depress the hysteresis error. Additionally, several auxiliary fixtures will be developed to control and fix the original cavity length and gauge length. It can improve the fabrication accuracy of the sensor and facility for the connection between the designed sensor and the measured target. This proposed sensor as a promising candidate can be expanded to many applications such as energy, aerospace, and gas turbines for strain measurement under harsh environment.

Funding

This work is supported by the National Science and Technology Major Project (2017-V-0003-0052) and the National Natural Science Foundation of China (Grant: 51905398), and partly supported by the Fundamental Research Funds for the Central Universities of China (Grant: 2020IVB027 and 2020III032GX).

Author Statement

Thanks for your and the reviewers' constructive comments on the manuscript (SNA_2020_1174R1). The authors have carefully read through the comments and made the corresponding revisions. The revisions in details and the updated manuscript (SNA_2020_1174R1) have been re-submitted to the Journal S̈ensors and Actuators A: Physicalv̈ia the online system.

The work is being proposed for publication uniquely to Sensors and Actuators A: Physical journal and is not under consideration elsewhere.

Thank you very much again for your kind attention, on behalf of all co-authors.

Declaration of Competing Interest

The authors declare that they have no known competing financial interests or personal relationships that could have appeared to influence the work reported in this paper.

References

[1] T. Sadowski, P. Golewski, Multidisciplinary analysis of the operational temperature increase of turbine blades in combustion engines by application of the ceramic thermal barrier coatings (TBC), Comput. Mater. Sci. 50 (2011) 1326–1335.
[2] N. Eliaz, G. Shemesh, R.M. Latanision, Hot corrosion in gas turbine components, Eng. Fail. Anal. 9 (2002) 31–43.
[3] W.H. Xie, S.H. Meng, H. Jin, C. Du, S.Y. Huo, L.B. Wang, et al., Measurement of high-temperature strains in superalloy and carbon/carbon composites using chemical composition gratings, Strain 53 (2017).
[4] R. Pollak, J. Lambros, Special issue on strain measurement in extreme environments, J. Strain Anal. Eng. 49 (2014) 202–203.
[5] X.W. Ye, Y.H. Su, J.P. Han, Structural health monitoring of civil infrastructure using optical Fiber sensing technology: a comprehensive review, Sci. World J. (2014).
[6] M.S. Hameed, I.A. Manarvi, Using FEM and CFD to locate cracks in compressor blades for non destructive inspections 2009 IEEE Aerospace Conference, Vols 1-7, 2009, pp. 2911–2921.
[7] T. Habisreuther, T. Elsmann, A. Graf, M.A. Schmidt, High-temperature strain sensing using sapphire fibers with inscribed first-order Bragg gratings, IEEE Photonics J. 8 (2016).
[8] A. Maskay, M.P. da Cunha, High-temperature static strain langasite SAWR sensor: temperature compensation and numerical calibration for direct strain reading, Sens. Actuator A-Phys. 259 (2017) 34–43.
[9] T.L. Li, Y.G. Tan, P. Xia, Z.D. Zhou, Paralleled structure-based string-type Fiber bragg grating acceleration sensor, IEEE Sens. J. 17 (2017) 1325–1332.
[10] Z. Chen, L. Yuan, G. Hefferman, T. Wei, Ultraweak intrinsic Fabry-Perot cavity array for distributed sensing, Opt. Lett. 40 (2015) 320–323.
[11] L. Xiong, Y. Guo, G. Jiang, X. Zhou, H. Liu, Six-dimensional force/torque sensor based on fiber Bragg gratings with low coupling, Ieee Trans. Ind. Electron. (2020) 1.
[12] D. Havermann, J. Mathew, W.N. MacPherson, R.R.J. Maier, D.P. Hand, Temperature and strain measurements with fiber Bragg gratings embedded in stainless steel 316, J. Lightwave Technol. 33 (2015) 2474–2479.
[13] D.C. Lee, J.J. Lee, I.B. Kwon, D.C. Seo, Monitoring of fatigue damage of composite structures by using embedded intensity-based optical fiber sensors, Smart Mater. Struct. 10 (2001) 285–292.
[14] M. Dvorak, H. Chlup, L. Horny, M. Ruzicka, Comparison of strain measurement methods: optical FBG sensors, strain gages & digital image correlation, Proceedings of the 50th Annual Conference on Experimental Stress Analysis (2012) 49–52.
[15] M. Deng, C.P. Tang, T. Zhu, Y.J. Rao, PCF-based Fabry-Perot interferometric sensor for strain measurement at high temperatures, IEEE Photonics Technol. Lett. 23 (2011) 700–702.
[16] Y. Huang, Z. Zhou, Y.N. Zhang, G.D. Chen, H. Xiao, A temperature self-compensated LPFG sensor for large strain measurements at high temperature, IEEE Trans. Instrum. Meas. 59 (2010) 2997–3004.
[17] M. Celikin, D. Barba, B. Bastola, A. Ruediger, F. Rosei, Development of regenerated fiber Bragg grating sensors with long-term stability, Opt. Express 24 (2016) 21897–21909.
[18] J. Canning, M. Stevenson, S. Bandyopadhyay, K. Cook, Extreme silica optical fibre gratings, Sensors (Basel) 8 (2008) 6448–6452.
[19] J. Habel, T. Boilard, J.S. Freniere, F. Trepanier, M. Bernier, Femtosecond FBG written through the coating for sensing applications, Sensors (Basel) 17 (2017).
[20] J. He, X.Z. Xu, C.R. Liao, C. Wang, Y.P. Wang, Femtosecond-laser-inscribed fiber Bragg gratings for high-tempertature sensing, 2018 Asia Communications and Photonics Conference (Acp) (2018).
[21] M. Lancry, K. Cook, J. Cao, T. Billotte, B. Poumellec, J. Canning, Study of stress relaxation in UV regenerated fiber Bragg gratings, 2017 Conference on Lasers and Electro-Optics Europe & European Quantum Electronics Conference (Cleo/Europe-Eqec) (2017).
[22] L.C. Zhang, Y. Jiang, H.C. Gao, J.S. Jia, Y. Cui, S.M. Wang, et al., Simultaneous measurements of temperature and pressure with a dual-cavity fabry-perot sensor, IEEE Photonics Technol. Lett. 31 (2019) 106–109.
[23] Y.J. Rao, T. Zhu, X.C. Yang, D.W. Duan, In-line fiber-optic etalon formed by hollow-core photonic crystal fiber, Opt. Lett. 32 (2007) 2662–2664.
[24] J. Villatoro, V. Finazzi, G. Coviello, V. Pruneri, Photonic-crystal-fiber-enabled micro-Fabry-Perot interferometer, Opt. Lett. 34 (2009) 2441–2443.
[25] F.C. Favero, L. Araujo, G. Bouwmans, V. Finazzi, J. Villatoro, V. Pruneri, Spheroidal Fabry-Perot microcavities in optical fibers for high-sensitivity sensing, Opt. Express 20 (2012) 7112–7118.
[26] S. Liu, Y.P. Wang, C.R. Liao, Z.Y. Li, K.M. Yang, High-sensitivity strain sensors based on in-fiber reshaped air bubbles, Proc. SPIE 9655 (2015).
[27] Y. Liu, C. Lang, X. Wei, S. Qu, Strain force sensor with ultra-high sensitivity based on fiber inline Fabry-Perot micro-cavity plugged by cantilever taper, Opt. Express 25 (2017) 7797–7806.
[28] S. Pevec, D. Donlagic, All-fiber, long-active-length Fabry-Perot strain sensor, Opt. Express 19 (2011) 15641–15651.
[29] A.M.R. Pinto, M. Lopez-Amo, Photonic crystal fibers for sensing applications, J Sensors (2012) 1–21.
[30] Y. Jiang, Fourier transform white-light interferometry for the measurement of fiber-optic extrinsic Fabry–Pérot interferometric sensors, IEEE Photonics Technol. 20 (2008) 75–77.
[31] E.G. Wolff, S.A. Eselun, Thermal expansion of a fused quartz tube in a dimensional stability test facility, Rev. Sci. Instrum. 50 (1979) 502.
[32] J. Oishi, T. Kimura, Thermal expansion of fused quartz, Metrologia 5 (1969) 50.

Biographies

Ping Xia is currently a PhD candidate at Wuhan University of Technology, China. Her research interests is high temperature optical fiber sensing technology and its application. She received her M.S. degree from Hubei University of Technology, China.

Yuegang Tan is currently a Professor with the School of Mechanical and Electronic Engineering, Wuhan University of Technology. His research interests include robot and its control, control theory and applications, and machinery equipment dynamic monitoring technology and application.

Tianliang Li (M'18) received the M.S and Ph.D. degree in mechanical engineering from Wuhan University of Technology, Wuhan, China, in 2014 and 2016. Dr. Li is currently a professor at School of Mechanical and Electronic Engineering, Wuhan University of Technology, Wuhan, China. He worked as a Research Fellow at Nanyang Technological University and the National University of Singapore, Singapore from 2016 to 2019. His research interests include optical fiber sensing and its applications, structure health monitoring, medical robotics sensing technologies. He is IEEE Member.

Zude Zhou is currently chair professor of School of Mechanical and Electronic Engineering, Wuhan University of Technology. His research interests include digital manufacturing, advanced manufacturing technology, digital monitoring and fault diagnosis, numerical control system &networked control system.

Wenqiang Lv is currently a Master candidate at Wuhan University of Technology, China.